RAPID COMMUNICATIONS

Boosted UV emission at 349 nm from mesoporous ZnS

P. Sajan · Junaid M. Bushiri · R. Vinod

Abstract Relatively oxygen-free mesoporous cubic ZnS particles were synthesised via a facile solvo-hydrothermal route using a water–acetonitrile combination. Boosted UV emission at 349 nm is observed from the ZnS prepared by the solvo-hydrothermal route. The increased intensity of this UV emission is attributed to activation of whispering gallery modes of almost elliptical microstructures made of porous nanostructures.

1 Introduction

Modern technology demands new UV sources especially for scintillation [1], for read heads to reduce data storage space, and for bio-imaging applications [2]. ZnS is a semiconductor material with large exciton binding energy of about 40 meV at room temperature [3]. Among the ZnS grown at different conditions, the cubic sphalerite phase has a band gap of the order of 3.68 eV, which is suitable to fabricate UV sources operating at ambient conditions [4–9]. ZnS is also best suited for biological systems and applications, since it is less toxic as compared to lead and cadmium compounds [10]. Even though there is a great interest in the photoluminescence (PL) properties of one-dimensional (1D) ZnS nanostructures, few studies are available in the literature on possible UV emission at room temperature. The reported UV emissions from ZnS are at 365 [11], 322 [12], 333 [13], 375 [14], 374 [15], and 380 nm [16], and these are have fewer applications

in device fabrication because of the feeble emission nature. Enhanced optical properties of ZnS nanocrystals are also obtained by using capping agents and surfactants like trioctylphosphine oxide (TOPO) [17], chitosan [18], trioctylphosphine oxide [19], ethylenediamine, dodecylthiol [20], 1-ethyl-3-methylimidazolium ethyl sulphate [21], and didecyldimethylammonium bromide (DDAB) [22] during the synthesis process. Even though the band-to-band edge emission of ZnS falls in the UV region, the majority of the chemically synthesised ZnS samples exhibit emission in the region 400–450 nm or, with doping, in the region 500–600 nm [23]. This is mainly due to high sensitivity of the 1D ZnS nanostructures' optical properties to the synthetic conditions.

More interestingly, mesoporous materials attained much attention because they possess more active sites with abundant inner spaces and surface area. These materials are likely to have better technological performance and are useful for applications in the fields of nanodevices, catalysts, sensors, medicines, drug delivery, etc. [24, 25]. The synthesis of mesoporous ZnS structures is achieved mostly by using surfactants as well as templates [24]. Xing et al. [25] used polyvinylpyrrolidone (PVP) and Zhang et al. [26] employed ethylene glycol as surfactants for the synthesis of mesoporous ZnS structures. A template-free solvothermal and hydrothermal method is also getting more attractive, because it is a low-cost method for the synthesis of large-scale materials [27]. In the hydrothermal synthesis process, water is used as solvent for reactants. But the presence of OH radicals in the water generally contributes to higher amounts of oxygen- and sulphur-related defects, which results in intense emission in the green and orange regions of the spectrum. So, this in turn will reduce the intensity of band-to-band UV emission.

P. Sajan · J.M. Bushiri (✉) · R. Vinod
Nanofunctional Materials Lab, Department of Physics, Cochin University of Science and Technology, Kochi 682022, Kerala, India
e-mail: junaidbushiri@gmail.com

2 Experimental

2.1 Synthesis

All the chemicals used for the present synthesis were AR grade. In the present work we used a water–acetonitrile solution combination as a solvent for solvo-hydrothermal reaction. ZnS crystals were synthesised by the reaction of zinc acetate, $Zn(CH_3COO)_2 \cdot 2H_2O$ (0.2 M), and Na_2S (1 M). Zinc acetate and Na_2S were taken in separate beakers and dissolved in 40 ml of water–acetonitrile solution (1:1 ratio), each separately. These solutions were allowed to dissolve by constant stirring using a magnetic stirrer for 5 min. Then the two solutions were mixed suddenly, stirred for 1 h, transferred to a Teflon-lined sealed stainless steel autoclave, and heated at 200 °C for a growth time of 12 h. After the heating process, the autoclave was allowed to cool naturally to room temperature. The precipitates were filtered out, washed with distilled water and ethanol, and dried in air atmosphere.

2.2 Characterization

The as-synthesised sample was characterized by a Rigaku D/Max-C X-ray diffractometer using Cu Kα radiation ($\lambda = 1.5418$ Å) with a scanning speed of 5°/min in the 2θ range 10–80°. The Raman spectrum of the sample was recorded with a Horiba Jobin Yvon LabRAM HR system with a He–Ne laser (632.8 nm) as the excitation source with a resolution better than 3 cm^{-1}. The morphological characterization and elemental analysis (Scanning Electron Microscopy-Energy Dispersive X-ray Spectroscopy (SEM-EDAX)) of the sample were carried out by a JEOL model JSM-6390LV and a JEOL model JED-2300. The transmission electron microscopy (TEM) images of the sample were recorded with a FEI Tecnai G^2 20 S-TWIN 200 keV transmission electron microscope. The UV-visible spectrum of the sample was recorded with a Jasco V-570 spectrometer in the wavelength range 220–800 nm and the room-temperature photoluminescence (PL) of the sample was recorded by a Horiba Jobin Yvon LabRAM HR system with a He–Cd laser (excitation wavelength 325 nm).

3 Results and discussion

Figure 1 shows the X-ray diffraction pattern recorded from the solvo-hydrothermally prepared ZnS sample. The X-ray diffraction pattern of the sample shows the formation of cubic sphalerite (zinc blende) ZnS phase (JCPDS 05-0566) with lattice constant $a = 5.4060$ Å [28].

Zinc blende structure of ZnS belongs to the T_d (43m) point group [29]. The first-order Raman spectra of zinc blende ZnS have transverse optical (TO) and longitudinal
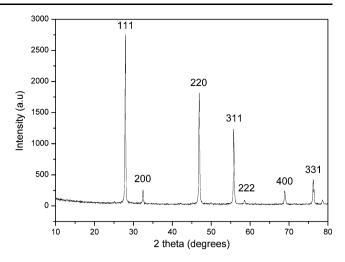

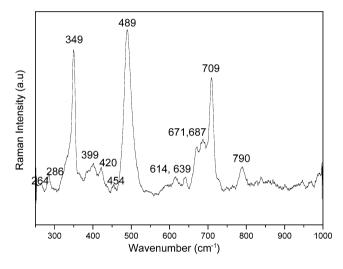**Fig. 1** XRD pattern of solvo-hydrothermally grown mesoporous ZnS at 200 °C

Fig. 2 Raman spectrum of solvo-hydrothermally grown mesoporous ZnS at 200 °C

optical (LO) modes, which lie below 1000 cm^{-1} [29]. In the present study we obtained Raman bands (Fig. 2) at 286 and 349 cm^{-1} corresponding to TO and LO zone-center phonons of cubic ZnS [30]. The weak nature of the Raman peak at 286 cm^{-1} confirms the cubic structure of the sample [30]. It is reported that both TO and LO modes of zinc blende structure are allowed for scattering from the (111) face only, TO mode from the (110) face only, and LO mode from the (100) face only [30]. In the X-ray diffraction pattern an intense peak at 27.9° indicates that the sample is highly crystalline and oriented in the (111) plane. In the present case both LO and TO modes contributing to the scattering from the (111) plane are seen, which is in agreement with our X-ray result.

The EDAX spectrum (Fig. 3) of the sample which shows the presence of only sulphur and zinc further supports our X-ray Diffraction (XRD) observation.

Figure 4a shows the SEM image of the ZnS sample prepared by using water as solvent and Fig. 4b shows the SEM image of the ZnS sample prepared by using water–acetonitrile (1:1 ratio) as solvent. From the SEM images, one can see that the morphology of the sample is getting spherical in nature and with less agglomeration when the water–acetonitrile combination is used. The particle size distribution histogram (shown in the inset of Fig. 4b) shows that the average particle size is around 265 nm.

Figures 5a, b, and c show the High Resolution Transmission electron microscopy (HRTEM) images of the prepared mesoporous ZnS sample and Fig. 5d depicts its Selected area electron diffraction (SAED) pattern. One can see the porous nature of the as-prepared material from the TEM images with pore size of about 2.4 nm.

Figure 6 shows the UV-visible absorption spectrum recorded from the prepared ZnS sample. The steep absorp-
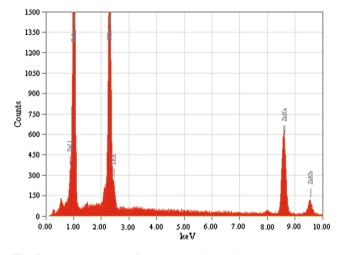
tion edge in the vicinity of 332–370 nm represents the transition between valence and conduction bands usually seen in direct band gap semiconductors like ZnS. Further, the observed absorption shoulder represents the presence of discontinuous energy levels in the band gap [28]. From the absorption spectrum of the sample, a sharp absorption edge is observed at 340 nm, which is the same as reported in bulk ZnS [31]. The band gap of the sample is calculated by using the Kubelka–Munk relation and is found to be 3.64 eV.

Figure 7 depicts the photoluminescence (PL) spectrum recorded from the as-prepared ZnS sample with an excitation wavelength of 325 nm. As reported in the literature, the PL emission in ZnS is contributed by different mechanisms, viz. near-band-edge (NBE) emission in the region 320–370 nm, which is known to originate from band-to-band transitions, or excitonic transitions or the quantum size effect. The violet (390 to 400 nm) emission is attributed to deep levels such as Zn^{2+} vacancies, S^{2-} interstitials, and dislocations. The blue (430–470 nm) emission is associated with the trapped luminescence arising from the Zn^{2+} and S^{2-} vacancies [32]. But the green (510–550 nm) emission is due to the presence of defect levels contributed by dopants or impurity atoms. The PL spectrum shows a highly intense emission peak in the UV region at 349 nm with a feeble shoulder peak at 336 nm and weak and broad profiles at 416 and 523 nm. The weak green emission at 523 nm from the sample under investigation can be associated with the electronic transfer from sulphur vacancies to its interstitial states [33]. The excitonic UV emission at 349 nm in the present sample is not reported so far in any of the ZnS structures. So, the present material has potential application in order to fabricate devices to emit 349 nm UV radiation [10].
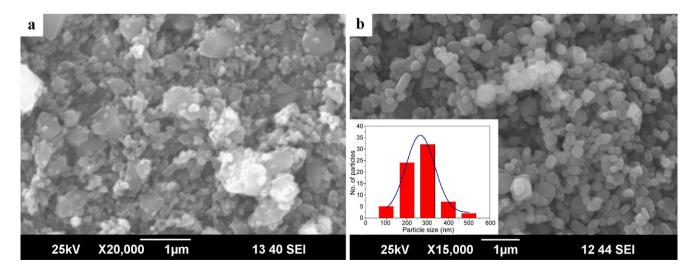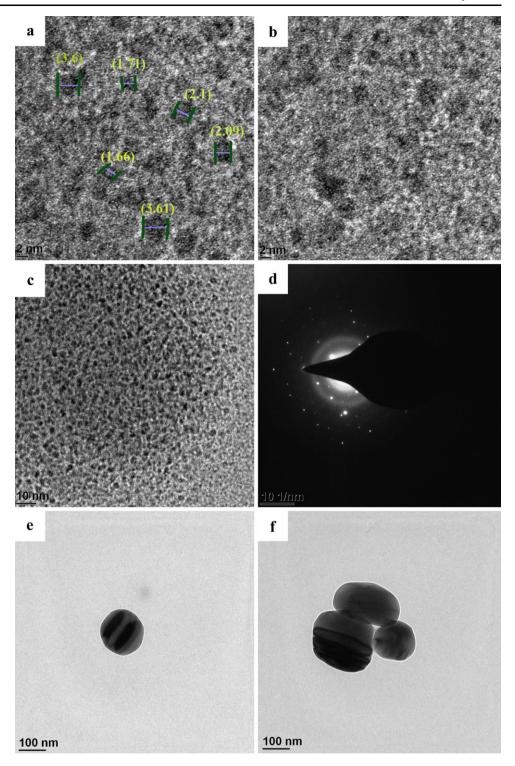

Fig. 3 EDAX spectrum of solvo-hydrothermally grown mesoporous ZnS at 200 °C

Fig. 4 SEM images of (**a**) hydrothermally grown ZnS, (**b**) solvo-hydrothermally grown mesoporous ZnS at 200 °C (*inset* shows the particle size distribution histogram)

Fig. 5 HRTEM images (**a**), (**b**), and (**c**) corresponds to magnified portion of micro-sized particles (**e**, and **f**), and (**d**) SAED pattern of solvohydrothermally synthesized mesoporous ZnS at 200 °C

4 Conclusions

In summary, we have synthesised almost oxygen-free mesoporous ZnS microspheres with an average pore size of around 2.4 nm. The average particle size is found to be about 265 nm from the histogram plotted based on the size distribution of particles in the SEM image. Our TEM observations with lower-resolution images show that the particles are elliptical in nature having an average diameter of the order of 0.1 to 0.15 μm by considering the dimensions of semi-major and semi-minor axes. These microstructures are made of mesoporous nanoregime structures which can generate UV radiation corresponding to their band gap when this system is suitably pumped by radiation having higher
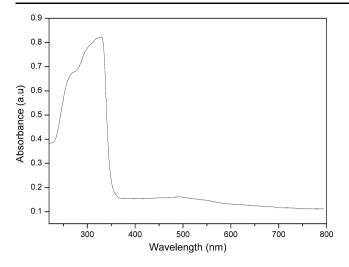
Fig. 6 Room temperature UV-visible absorption spectrum of solvo-hydrothermally synthesised mesoporous ZnS at 200 °C
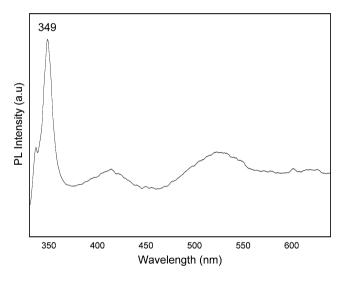

Fig. 7 Room temperature photoluminescence spectrum of mesoporous ZnS grown at 200 °C

frequency. Thus, the generated UV radiation will be amplified by the whispering gallery modes (WGMs) of the elliptical microstructures [34]. So, the unusual enhancement in the UV radiation at 349 nm is partially contributed by WGM activation of the ZnS microstructures. The present material can be used for bio-imaging, in the medical field, as well as in fabricating UV lasers and LEDs. Furthermore, this material is helpful to excite important bio-molecules like nicotinamide adenine dinucleotide (NADH-4, which is an important cell metabolism indicator).

References

1. S.R. Choube, S.C. Gedam, S.J. Dhoble, Recent Res. Sci. Technol. **4**(8), 75 (2012)
2. S.K. Mehta, S. Kumar, J. Lumin. **130**, 2377 (2010)
3. T.K. Tran, W. Park, W. Tong, M.M. Kyi, B.K. Wagner, C.J. Summers, J. Appl. Phys. **81**, 2803 (1997)
4. H. Fujiwara, H. Hosokawa, K. Murakoshi, Y. Wada, S. Yanagida, Langmuir **14**, 5154 (1998)
5. H. Li, R. Brescia, R. Krahne, G. Bertoni, M.J.P. Alcocer, C. D'Andrea, F. Scotognella, F. Tassone, M. Zanella, M. De Giorgi, L. Manna, ACS Nano **6**(2), 1637 (2012)
6. J. Xu, W. Ji, J. Mater. Sci. Lett. **18**, 115 (1999)
7. L. Sun, C. Liu, C. Liao, C. Yan, J. Mater. Chem. **9**, 1655 (1999)
8. G.H. Yue, P.X. Yan, D. Yan, X.Y. Fan, M.X. Wang, D.M. Qu, J.Z. Liu, Appl. Phys. A **84**, 409 (2006)
9. J.A. Zapien, Y. Jiang, X.M. Meng, W. Chen, F.C.K. Au, Y. Lifshitz, S.T. Lee, Appl. Phys. Lett. **84**, 1189 (2004)
10. A. Chatterjee, A. Priyam, S.C. Bhattacharya, A. Saha, Colloids Surf. A, Physicochem. Eng. Asp. **297**, 258 (2007)
11. B. Bodo, R. Singha, S.C. Das, Int. J. Appl. Phys. Math. **2**(4), 287 (2012)
12. C. Cheng, G. Xu, H. Zhang, J. Cao, P. Jiao, X. Wang, Mater. Lett. **60**, 3561 (2006)
13. X.M. Meng, J. Liu, Y. Jiang, W.W. Chen, C.S. Lee, I. Bello, S.T. Lee, Chem. Phys. Lett. **382**, 434 (2003)
14. W.S. Chae, J.H. Yoon, H. Yu, D.J. Jang, Y.R. Kim, J. Phys. Chem. B **108**, 31 (2004)
15. H.J. Yuan, S.S. Xie, D.F. Liu, X.Q. Yan, Z.P. Zhou, L.J. Ci, J.X. Wang, Y. Gao, L. Song, L.F. Liu, W.Y. Zhou, G. Wang, J. Cryst. Growth **258**, 225 (2003)
16. J. Li, D. Zhao, X. Meng, Z. Zhang, J. Zhang, D. Shen, Y. Lu, X. Fan, J. Phys. Chem. B **110**, 14685 (2006)
17. M.A. Malik, P. O'Brien, N. Revaprasadu, J. Mater. Chem. **11**, 2382 (2001)
18. M. Sharma, S. Singh, O.P. Pandey, J. Appl. Phys. **107**, 104319 (2010)
19. L. Manna, E.C. Scher, L.S. Li, A.P. Alivisatos, J. Am. Chem. Soc. **124**, 7136 (2002)
20. Q. Zhao, L. Hou, R. Huang, Inorg. Chem. Commun. **6**, 971 (2003)
21. V. Taghvaei, A.H. Yangjeh, M. Behboudnia, Physica E **42**, 1973 (2010)
22. G. Li, J. Zhai, D. Li, X. Fang, H. Jiang, Q. Dong, E. Wang, J. Mater. Chem. **20**, 9215 (2010)
23. X. Zhang, Y. Zhang, Y. Song, Z. Wang, D. Yu, Physica E **28**, 1 (2005)
24. K. Xue, D. Chen, X. Jiao, Inorg. Chem. **49**, 1191 (2010)
25. R. Xing, Y. Xue, X. Liu, B. Liu, B. Miao, W. Kanga, S. Liu, CrystEngComm **14**, 8044 (2012)
26. Q. Zhang, W. Chi, W. Zhang, C. Lv, J. Li, New J. Chem. **36**, 119 (2012)
27. M. Muruganandham, R. Amutha, E. Repo, M. Sillanpaa, Y. Kosumoto, M.A. Al-Mamun, J. Photochem. Photobiol. A, Chem. **216**, 133 (2010)
28. Y. Li, A. Lu, C. Wang, X. Wu, Sol. Energy Mater. Sol. Cells **92**, 953 (2008)
29. Y.C. Cheng, C.Q. Jin, F. Gao, X.L. Wu, W. Zhong, S.H. Li, P.K. Chu, J. Appl. Phys. **106**, 123505 (2009)
30. S.S. Kumar, M.A. Khadar, S.K. Dhara, T.R. Ravindran, K.G.M. Nair, Nucl. Instrum. Methods Phys. Res. B **251**, 435 (2006)
31. L. Peng, Y. Wang, Nanoscale Res. Lett. **5**, 839 (2010)
32. S. Park, C. Jin, H. Kim, C. Hong, C. Lee, J. Lumin. **132**, 231 (2012)
33. X. Wang, J. Shi, Z. Feng, M. Li, C. Li, Phys. Chem. Chem. Phys. **13**, 4715 (2011)
34. K. Okazaki, T. Shimogaki, K. Fusazaki, M. Higashihata, D. Nakamura, N. Koshizaki, T. Okada, Appl. Phys. Lett. **101**, 211105 (2012)